Biogeosciences, 13, 3991–4004, 2016
www.biogeosciences.net/13/3991/2016/
doi:10.5194/bg-13-3991-2016

Biogeosciences Open Access EGU

Analysing the uncertainty of estimating forest carbon stocks in China

Tian Xiang Yue[1,2,3], Yi Fu Wang[4], Zheng Ping Du[1], Ming Wei Zhao[1,2], Li Li Zhang[1,2], Na Zhao[1,2,3], Ming Lu[1,2], Guy R. Larocque[5], and John P. Wilson[6]

[1]State Key Laboratory of Resources and Environment Information System, Institute of Geographical Science and Natural Resources Research, Beijing 100101, China
[2]College of Resources and Environment, University of Chinese Academy of Sciences, Beijing 100049, China
[3]Jiangsu Center for Collaborative Innovation in Geographical Information Resource Development and Application, Nanjing 210023, China
[4]College of Forestry, Beijing Forestry University, Beijing 100083, China
[5]Natural Resources Canada, Canadian Forest Service, Laurentian Forestry Centre, Québec (QC), G1V 5B9, Canada
[6]6Spatial Sciences Institute, Dana and David Dornsife College of Letters, Arts and Sciences, University of Southern California, Los Angeles, CA 90089-0374, USA

Correspondence to: Tian Xiang Yue (yue@lreis.ac.cn) and Yi Fu Wang (wangyf@lreis.ac.cn)

Received: 16 October 2015 – Published in Biogeosciences Discuss.: 10 December 2015
Revised: 12 June 2016 – Accepted: 14 June 2016 – Published: 12 July 2016

Abstract. Earth surface systems are controlled by a combination of global and local factors, which cannot be understood without accounting for both the local and global components. The system dynamics cannot be recovered from the global or local controls alone. Ground forest inventory is able to accurately estimate forest carbon stocks in sample plots, but these sample plots are too sparse to support the spatial simulation of carbon stocks with required accuracy. Satellite observation is an important source of global information for the simulation of carbon stocks. Satellite remote sensing can supply spatially continuous information about the surface of forest carbon stocks, which is impossible from ground-based investigations, but their description has considerable uncertainty. In this paper, we validated the Kriging method for spatial interpolation of ground sample plots and a satellite-observation-based approach as well as an approach for fusing the ground sample plots with satellite observations. The validation results indicated that the data fusion approach reduced the uncertainty of estimating carbon stocks. The data fusion had the lowest uncertainty by using an existing method for high-accuracy surface modelling to fuse the ground sample plots with the satellite observations (HASM-S). The estimates produced with HASM-S were 26.1 and 28.4 % more accurate than the satellite-based approach and spatial interpolation of the sample plots respectively. Forest carbon stocks of 7.08 Pg were estimated for China during the period from 2004 to 2008, an increase of 2.24 Pg from 1984 to 2008, using the preferred HASM-S method.

1 Introduction

Biomass dynamics reflects the potential of vegetation to act as a carbon sink over the long term, as they integrate photosynthesis, autotrophic respiration and litter fall fluxes (Thurner et al., 2014). Forest ecosystems cover more than 41 million km^2 of the Earth's land surface and forests are thought to contain about half of the carbon in terrestrial biomes (Prentice et al., 2001). Forests play an important role in the active mitigation of atmospheric CO_2 through increased carbon stocks. The fixation of atmospheric CO_2 into plant tissue through photosynthesis is one of the most effective mechanisms for offsetting carbon emissions (Canadell and Raupach, 2008; Gonzalez-Benecke et al., 2010).

Carbon sequestration by trees is the best way to store a large amount of terrestrial carbon over long durations (Jung et al., 2013). Estimation of carbon stocks at scales ranging from local to global is crucial for accurately predicting fu-

ture changes in atmospheric carbon dioxide (Yu et al., 2014). However, substantial uncertainties remain in current model estimates of terrestrial carbon and there is an increasing need to quantify and reduce these uncertainties (Barman et al., 2014; Ahlstroem et al., 2012).

Several studies have estimated the forest carbon stocks in China. Piao et al. (2005), on the one hand, used a satellite-based approach and estimated that (1) the total forest biomass of China averaged 5.79 Pg C during the period 1981–1999, with an average biomass density of 4.531 kg C m^{-2}; and (2) the total forest biomass C stock increased from 5.62 Pg C in the early 1980s to 5.99 Pg C by the end of the 1990s, giving a total increase of 0.37 Pg C and an annual sequestration rate of 0.019 Pg C yr^{-1}. Zhang et al. (2007), on the other hand, analysed seven forest inventories from 1973 to 2008 and suggested that the total biomass carbon stocks (BCDs) of all forest types increased by 65 % during this period, reaching 8.12 Pg C in 2008.

Wang et al. (2007) used the Integrated Terrestrial Ecosystem C-budget model and estimated that China's forests were a source of 21.0 ± 7.8 Tg C yr^{-1} due to human activities during the period 1901–1949 and that this flux increased to 122.3 ± 25.3 Tg C yr^{-1} due to intensified human activities during the period 1950–1987. However, these forests became large sinks of 176.7 ± 44.8 Tg C yr^{-1} during the period 1988–2001 owing to large-scale plantation and forest regrowth in previously disturbed areas (see the description of the Grain for Green Program below) as well as climatic warming, atmospheric CO_2 fertilization, and N deposition.

Yang and Guan (2008) utilized the continuous biomass expansion factor (BEF) method with field measurements of forests plots in different age classes and forest inventory data; they showed that the carbon density of the forests in the Pearl River Delta increased by 14.3 % from 19.08 to 21.81 kg C m^{-2} during the period 1989–2003. Similarly, Piao et al. (2009) reported that China's terrestrial ecosystems were a net carbon sink of 0.19–0.26 Pg carbon per year and that they absorbed 28–37 % of the fossil carbon emissions during the 1980s and 1990s. However, their results also showed that northeastern China is a net source of CO_2 to the atmosphere due to the over-harvesting and degradation of forests, while southern China accounts for more than 65 % of the carbon sink, which can be attributed to regional climate change, large-scale plantation programs initiated in the 1980s, and shrub recovery (Piao et al., 2009).

Guo et al. (2010) used three different approaches – the mean biomass density (MBD) method, the mean ratio (MR) method, and the continuous BEF method (CBM) – with forest inventory data to estimate China's forest biomass C stocks and their changes from 1984 to 2003. The MBD, MR, and CBM estimated that forest biomass C stocks increased from 5.7 to 7.7, 4.2 to 6.2, and 4.0 to 5.9 Pg C respectively.

Deng et al. (2011) deployed a GIS approach and defined the vegetation carbon sink as the carbon sequestration from the atmosphere ($1.63 \times$ NPP), the vegetation carbon stock as the carbon content that aboveground vegetation holds, and the soil carbon stock as the carbon content that soil organic matter holds. These authors estimated vegetation and soil carbon stocks to 1.58 and 1.41 Pg C respectively in the forest ecosystems of China for the period 1981–2000.

Ni (2013) used available national-scale information to estimate that (1) the mean vegetation carbon in China was 36.98 Pg and mean soil carbon was 100.75 Pg C and (2) the forest and grassland sectors supported mean carbon stocks of 5.49 and 1.41 Pg C respectively.

The aforementioned studies show that the forest ecosystems of China store steadily increasing stocks of carbon and that these forest stands have great potential to absorb more biomass carbon in the future due to large fractions of young and middle-aged forests and programs to promote the conservation of soil and biological resources.

All these published results, which relied on either ground- or satellite-observation-based (SOA) estimation, resulted in pronounced differences in carbon stock estimates. The objective of this study was to evaluate whether fusing these data sources could reduce the uncertainty associated with the final carbon stock estimates.

2 Data and materials

The forest distribution data were created by combining the Vegetation Map of the People's Republic of China (Editorial Committee of Vegetation Map of China, 2007) with a vegetation map produced from the forest inventory conducted during the period from 2004 to 2008 (State Forestry Administration of China, 2009). The former provides a detailed classification of plant functional types and describes the phenological and regional character of forests in China, but it is not so exact. The latter shows the forest distribution in the period of the forest inventory, but its classification provides less information about plant functional types. The combination of the two kinds of maps retains the advantages of both.

The forest distribution data covers 161 plant biomes, including 5 classes of deciduous needle-leaved trees, 57 classes of evergreen needle-leaved trees, 39 classes of deciduous broad-leaved trees, 56 classes of evergreen broad-leaved trees, and 4 classes of mixed trees (Fig. 1).

The national forestry inventory database (FID) for the period 2004–2008 includes 160 000 permanent sample plots and 90 000 temporary sample plots scattered across China. The biomass density of each forest type in each province was calculated from timber volume, using a BEF (Fang et al., 2007). The biomass carbon density (BCD) of each forest type in each province was calculated next by multiplying the biomass density by a carbon factor (CF) (Li and Lei, 2010). Finally, the BCS of each forest type in each province was calculated by multiplying the BCD by the area of that forest type. The total BCS in China is a sum of the BCS of all of the

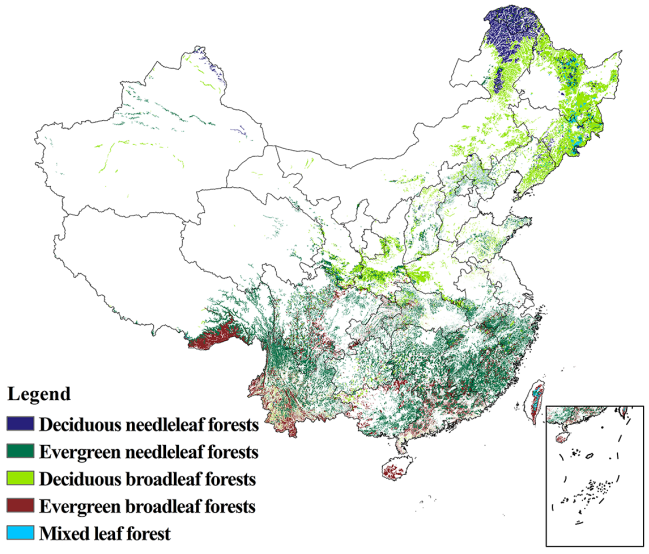

Figure 1. The forest cover map of China.

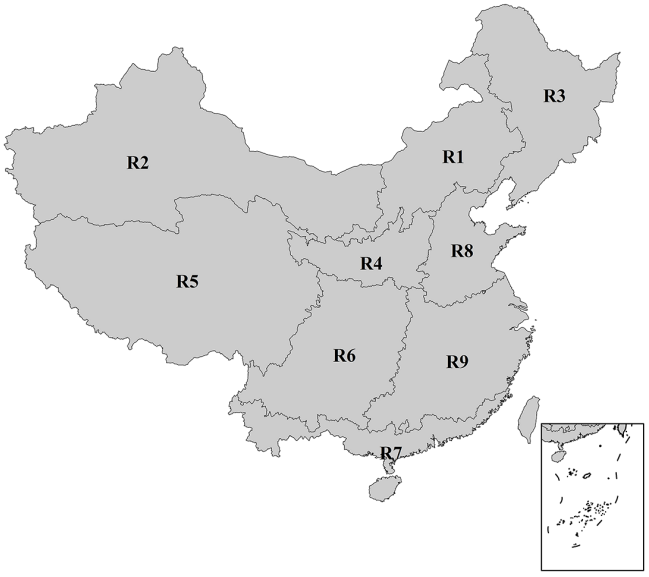

Figure 2. Map showing the nine regions of China used for detailed analysis.

forest types in the 31 provinces of China, excluding Taiwan, Hong Kong, and Macao.

The following formulations were used to calculate the forest BCS in China:

$$\mathrm{TCS} = \sum_{i=1}^{M}\sum_{j=1}^{N}\left(A_{i,j}\mathrm{BCD}_{i,j}\right) \times 10^{-12}, \quad (1)$$

$$\mathrm{BCD}_{i,j} = W_{i,j} \times \mathrm{CF}_i, \quad (2)$$

$$W_{i,j} = \mathrm{BEF}_i \times V_{i,j}, \quad (3)$$

$$\mathrm{BEF}_{i,j} = a_i + \frac{b_i}{V_{i,j}}, \quad (4)$$

where TCS is the total forest BCSs of China (Pg); $\mathrm{BCD}_{i,j}$ is the area weighted biomass carbon density of the ith forest type in the jth province ($\mathrm{kg\,m^{-2}}$); $A_{i,j}$ is the area of the ith forest type in the jth province ($\mathrm{m^2}$); M and N refer to the numbers of forest types and provinces in China respectively; $W_{i,j}$ is the area weighted mean forest biomass of the ith forest type in the jth province ($\mathrm{kg\,m^{-2}}$); CF_i is the CF of the ith forest type; $V_{i,j}$ is the area weighted mean timber volume of the ith forest type in the jth province ($\mathrm{m^3\,m^{-2}}$); BEF_i is the BEF of the ith forest type ($\mathrm{kg\,m^{-3}}$); and a_i ($\mathrm{kg\,m^{-3}}$) and b_i($\mathrm{kg\,m^{-2}}$) are constants of the ith forest type to be simulated. The mean CF_i of all coniferous forest types was used for coniferous mixed forest. The mean CF_i of all broad-leaved forest types was used for broad-leaved mixed forest. The mean CF_i of all broad-leaved and coniferous forest types was used for broad-leaved and coniferous mixed forest.

The land mass of China was next divided into nine regions (Fig. 2) with similar temperature, precipitation and soil regimes to make it easier to analyse changes in forest carbon storage from one place to another (Zhou et al., 1981). The nine regions are referred to as R_k, where $k = 1$ to 9 and we use periods 1, 2, 3, 4, and 5 to represent the periods 1984–1988, 1989–1993, 1994–1998, 1999–2003, and 2004–2008 respectively.

3 Methods

3.1 Satellite-observation-based approach

The SOA used the Normalized Differential Vegetation Index (NDVI) at a temporal resolution of 1 month and at a spatial resolution of 1 km × 1 km from the Earth Observation System's Moderate Resolution Imaging Spectroradiometer (EOS MODIS) (Piao et al., 2009). The BCD from the FID data was matched with the NDVI data using the forest map of China reproduced in Fig. 1.

The BCD mirrored the latitude, longitude, and maximum value of the monthly-averaged NDVI values during the seventh national forest inventory conducted from 2004 to 2008:

$$\begin{aligned}\mathrm{BCD}_j &= 93.351\ln(\mathrm{NDVI}_j)\\ &-2.96\,\mathrm{Lat}_j - 21.388\,\mathrm{Long}_j\\ &+0.047\,\mathrm{Lat}_j^2 + 0.091\,\mathrm{Long}_j^2 + 1339.03,\end{aligned} \quad (5)$$

where NDVI_j is the mean of the maximum values of the monthly-averaged NDVI values during the period 2004–2008 in the jth province, and Lat_j and Long_j refer to the latitude and longitude of the centre of the jth province respectively. The coefficient of correlation ($R = 0.91$) and significance ($P < 0.001$) show how latitude, longitude, and NDVI explained 83 % of the variability in BCD.

3.2 High-accuracy surface modelling (HASM)

HASM was developed for efficiently fusing satellite with ground observations to find solutions for error problems which have long troubled Earth surface modelling (Yue, 2011). HASM has been successfully used to construct digital elevation models (Yue et al., 2007, 2010a, b; Yue and Wang, 2010; Chen and Yue, 2010; Chen et al., 2013a, b), model surface soil properties (Shi et al., 2011) and soil pollution (Shi et al., 2009), fill voids in the Shuttle Radar Topography Mission (SRTM) dataset (Yue et al., 2012), simulate climate change (Yue et al., 2013a, b; Zhao and Yue, 2014a, b), fill voids in remotely sensed XCO_2 surfaces (Yue et al., 2015a), and analyse ecosystem responses to climatic change (Yue et al., 2015b). In all of these applications, HASM produced more accurate results than the classical methods (Yue et al., 2015c).

3.3 Estimation of carbon stocks

Forest carbon stocks and carbon densities were estimated by methods of spatial interpolation, SOA, and data fusion. The spatial interpolation provided an effective approach to construct a continuous surface from the FID by means of Kriging; it took advantage of limited observation data to estimate the most plausible spatial distribution by filling in missing data. The data fusion approach integrated the forest inventory and satellite data into a consistent, accurate, and useful representation using HASM (HASM-S) (see Supplement 1 in details); the aim of the data fusion was to improve the quality of the information so that it was more accurate than would be possible had the data sources been used individually.

3.4 Validation

The uncertainties of the carbon stock estimates reported in earlier studies relied on several different concepts and metrics. The same formula for absolute and relative error should be used to evaluate all estimates of carbon stocks so that the estimation results are comparable. We calculated the mean absolute errors (MAEs) and mean relative errors (MREs) respectively, as

$$\mathrm{MAE} = \frac{1}{n}\sum_{i}^{n}|o_i - s_i|, \tag{6}$$

$$\mathrm{MRE} = \frac{\mathrm{MAE}}{\frac{1}{n}\sum_{i}^{n}|o_i,|} \tag{7}$$

where o_i represents the forest carbon stocks at the ith control point, s_i represents the simulated value at the ith control point, and n is the total number of control points used for validation.

Cross-validation is used to estimate how accurately a model performs, which is analysed by removing certain data points in turn and summing the absolute value of the discrepancy of each removed data point from the simulated one at the same location (Hulme et al., 1995). It was comprised of four steps: (1) 5 % of the sample plots from the national forest inventory were removed for validation. (2) The spatial distribution of average forest BCSs in China during the period 2004–2008 were simulated at a spatial resolution of 5 km × 5 km using the remaining 95 % of the sample plots from the national forest inventory by means of the different methods. (3) The MAEs and MREs were calculated using the 5 % validation set. (4) The 5 % validation set was returned to the pool for the next iteration, and another 5 % validation set was removed. This final process was repeated until all the sample plots were used for validation at least one time and the simulation error statistics could be calculated for each sample plot.

4 Results

The three maps of mean annual carbon stocks during the period 2004–2008 reproduced with each of the aforementioned methods show how the Kriging, SOA, and HASM-S methods were able to generate the same overall patterns based on the underlying forest cover and how the estimates varied using each of these methods over large parts of the China (Fig. 3). This variability raises questions related to the reliability of the estimates produced with the three aforementioned approaches.

The cross-validation results indicated that Kriging and SOA had larger errors, with MREs of 50.12 and 48.77 % respectively. Kriging overestimated the carbon stocks, while SOA underestimated the carbon stocks (Table 1). Accuracy was considerably improved when the forest inventory and satellite data were fused by using HASM-S. The MRE of HASM-S was 22.71 %.

The BCSs of all forest types estimated with HASM-S (the best approach) was 7.08 Pg in China during the period 2004–2008. The BCSs of coniferous, broad-leaved, and mixed forests were 2.74, 3.95, and 0.39 Pg respectively (Table 1). The mean biomass carbon densities (MBCDs) of the coniferous, broad-leaved, and mixed forests were 4.35, 4.74, and 4.20 kg m^{-2} respectively.

The HASM-S estimates showed that 89.9 % of the MBCDs were found in the regions R5, R3, R6, R9, and R7 during the period P5, accounting for 28.61, 28.41, 14.48, 12.52, and 5.89 % of the BCSs respectively. The three largest BCDs occurred in R5 (Tibetan Plateau; 10.53 kg m^{-2}), R2 (arid area; 6.33 kg m^{-2}), and R3 (northeastern China; 4.44 kg m^{-2}) (Table 2 and Fig. 3c). The two smallest BCDs were predicted in the R8 (2.14 kg m^{-2}) and R9 (2.60 kg m^{-2}) regions.

The HASM-S estimates can be parsed by forest type as well (Table 3). Hence, the BCDs of evergreen broad-leaved and evergreen coniferous forests were 6.23 and 4.47 kg m^{-2}

Table 1. Biomass carbon stocks and biomass carbon densities as well as their errors produced by different methods.

Method	Calculated object	Coniferous forests	Mixed forests	Broad-leaved forests	Total	MAE ($kg\,m^{-2}$)	MRE (%)
SOA	BCS (Pg)	2.48	0.46	3.61	6.55	1.92	48.77
	BCD ($kg\,m^{-2}$)	3.94	4.93	4.34			
Kriging	BCS (Pg)	2.76	0.39	4.11	7.26	1.97	50.12
	BCD ($kg\,m^{-2}$)	4.38	4.24	4.94			
HASM-S	BCS (Pg)	2.74	0.39	3.95	7.08	0.89	22.71
	BCD ($kg\,m^{-2}$)	4.35	4.2	4.74			

Table 2. BCS and BCD of the forests in the nine regions of China during the periods 2004–2008 and 1984–1988.

Regions	P5 (from 2004 to 2008)			P1 (from 1984 to 1988)		
	BCD ($kg \times m^{-2}$)	BCS (Pg)	Percentage (%)	BCD ($kg \times m^{-2}$)	BCS (Pg)	BCS accumulation rate ($Tg \times yr^{-1}$)
R1	3.710	0.28	3.94	2.666	0.16	6.2
R2	6.330	0.20	2.80	6.358	0.15	2.3
R3	4.445	2.01	28.41	4.493	1.59	21.3
R4	3.274	0.19	2.68	3.035	0.13	2.8
R5	10.525	2.03	28.61	6.718	0.99	52.0
R6	3.671	1.03	14.48	3.734	0.82	10.4
R7	3.693	0.42	5.89	3.643	0.36	2.9
R8	2.138	0.06	0.83	1.515	0.03	1.3
R9	2.598	0.87	12.26	2.358	0.62	12.7
Total		7.08	100		4.84	112

respectively, while the BCDs for deciduous broad-leaved and deciduous coniferous forests were 3.93 and 3.77 $kg\,m^{-2}$ respectively in P5. The BCD of evergreen forests was 50 % larger than that of deciduous forests, and the BCDs for broad-leaved forests were greater than those for both coniferous and deciduous forests. Turning next to the BCSs, the evergreen coniferous forests contributed the largest proportion, accounting for 33.05 %, followed by deciduous broad-leaved forests (29.8 %) and evergreen broad-leaved forests (25.99 %). The deciduous coniferous and the broad-leaved and coniferous mixed forests accounted for the two smallest proportions of the total BCS, 5.65 and 5.51 % respectively.

The HASM-S estimates also indicate that BCSs rose from 4.84 Pg in period 1 to 7.08 Pg in P5 due to the increase of BCD and the expansion of forest area (Table 4). The BCD rose from 4.00 $kg\,m^{-2}$ in P1 to 4.55 $kg\,m^{-2}$ in P5 and the forest area grew from 1.21 million km^2 in P1 to 1.56 million km^2 in P5. The increasing trends of the BCS, BCD, and forest area (FA) are captured by the following regression equations:

$$\mathrm{BCS}(t) = 0.531t + 4.297 \quad R = 0.976, \tag{8}$$

$$\mathrm{BCD}(t) = 0.125t + 3.958 \quad R = 0.943, \tag{9}$$

$$\mathrm{FA}(t) = 0.083t + 1.1045 \quad R = 0.96, \tag{10}$$

where t corresponds to periods 1, 2, 3, 4, and 5; BCS(t), BCD(t), and FA(t) are BCS, BCD, and FA respectively in the period t; and R represents the correlation coefficient for the corresponding regression equation.

Although BCS rose in all nine regions from period 1 to 5, the spatial variability over China more or less mirrors the variability in the distribution of forests (Figs. 4, 5, Table 4). For regions R1 and R8, for example, both BCS and BCD have continuously increased from period 1 to 5. R8 has the smallest BCS, which only accounted for 0.83 % of the BCS of the whole of China, and the smallest BCD of 2.14 $kg\,m^{-2}$ in P5 as well as the lowest BCS accumulation rate of 1.3 $Tg \times yr^{-1}$. In R1, BCS accounted for 3.94 % of the total BCS of China for the period of P5 and the BCS accumulation rate has averaged 6.2 $Tg \times yr^{-1}$ from P1 to P5.

The region R5 had the largest BCS, accounting for 28.61 % of the total BCS of China in P5, along with the largest BCD of 10.53 $kg\,m^{-2}$ and the fastest BCS accumulation rate of 52 $Tg \times yr^{-1}$; the BCS has shown a monotonically increasing trend since P1. The second largest BCS oc-

Table 3. BCSs and BCDs for all forest types during the five periods estimated using HASM-S.

Period	Calculation object	Deciduous coniferous forests	Evergreen coniferous forests	Broad-leaved and coniferous mixed forests	Deciduous broad-leaved forests	Evergreen broad-leaved forests
P1	BCS (Pg)	0.41	1.50	0.06	1.38	0.63
	BCD ($kg\,m^{-2}$)	4.35	3.81	3.08	3.75	4.35
P2	BCS (Pg)	0.39	1.80	0.09	1.44	0.87
	BCD ($kg\,m^{-2}$)	4.28	4.13	3.75	3.77	5.65
P3	BCS (Pg)	0.44	2.23	0.07	1.66	1.20
	BCD ($kg\,m^{-2}$)	4.20	4.09	3.03	3.87	6.35
P4	BCS (Pg)	0.47	2.19	0.19	1.97	1.57
	BCD ($kg\,m^{-2}$)	4.37	4.40	5.18	3.89	7.49
P5	BCS (Pg)	0.40	2.34	0.39	2.11	1.84
	BCD ($kg\,m^{-2}$)	3.77	4.47	4.20	3.93	6.22

Table 4. Biomass carbon stocks and biomass carbon densities estimated by HASM-S.

Regions	Calculation object	Period 1	Period 2	Period 3	Period 4	Period 5
R1	BCS (Pg)	0.16	0.17	0.17	0.2	0.28
	BCD ($kg\,m^{-2}$)	2.67	2.71	2.88	2.98	3.71
R2	BCS (Pg)	0.15	0.16	0.15	0.18	0.2
	BCD ($kg\,m^{-2}$)	6.36	6.27	6.25	6.23	6.33
R3	BCS (Pg)	1.59	1.64	1.64	1.77	2.01
	BCD ($kg\,m^{-2}$)	4.49	4.42	4.5	4.43	4.44
R4	BCS (Pg)	0.13	0.15	0.14	0.16	0.19
	BCD ($kg\,m^{-2}$)	3.04	3.23	3.13	3.15	3.27
R5	BCS (Pg)	0.99	1.57	1.64	1.94	2.03
	BCD ($kg\,m^{-2}$)	6.72	10.15	10.83	11.49	10.53
R6	BCS (Pg)	0.82	0.87	0.82	0.96	1.03
	BCD ($kg\,m^{-2}$)	3.73	3.78	3.66	3.88	3.67
R7	BCS (Pg)	0.36	0.39	0.37	0.4	0.42
	BCD ($kg\,m^{-2}$)	3.64	3.79	3.66	3.54	3.69
R8	BCS (Pg)	0.03	0.04	0.04	0.05	0.06
	BCD ($kg\,m^{-2}$)	1.52	1.64	1.89	1.89	2.14
R9	BCS (Pg)	0.62	0.56	0.62	0.73	0.87
	BCD ($kg\,m^{-2}$)	2.36	2.05	2.3	2.51	2.6
The whole of China	BCS (Pg)	4.84	5.55	5.6	6.38	7.08
	BCD ($kg\,m^{-2}$)	4	4.32	4.33	4.47	4.55
	Area (million km^2)	1.2101	1.2864	1.292	1.4279	1.5559

curred in R3 (northeastern China). The BCS in R3 accounted for 28.41 % of the total BCS of China. However, the BCD in R3 has declined since P3 following increases from P1 to P2 and from P2 to P3. The mean BCS accumulation rate in R3 was 21.3 $Tg\,yr^{-1}$.

In the regions R4 (Loess Plateau), R6, and R9, both BCS and BCD have increased since P3. The BCSs in R4, R6, and R9 accounted for 2.68, 14.48, and 12.26 % of the BCS in the whole of China in P5 respectively. The average BCS accumulation rates were 2.8, 10.4, and 12.7 $Tg \times yr^{-1}$ respectively in R4, R6, and R9. In R2 (an arid area), the BCS accounted for 2.80 % of the total for China in the period P5. The BCS and BCD increased from P4 to P5, but the mean accumulation rate of BCS was only 2.3 $Tg \times yr^{-1}$. The BCS accounted for 5.89 % of the total for China in R7. The BCS and BCD both increased from P4 to P5 but, like in R2, the mean BCS accumulation rate was relatively low at just 2.9 $Pg \times yr^{-1}$.

In terms of forest types, evergreen broad-leaved forests had the fastest BCS accumulation rate and the largest BCD, while evergreen coniferous forests contributed the largest BCS. The BCSs of broad-leaved forests increased during all five periods. The BCS of evergreen broad-leaved forests

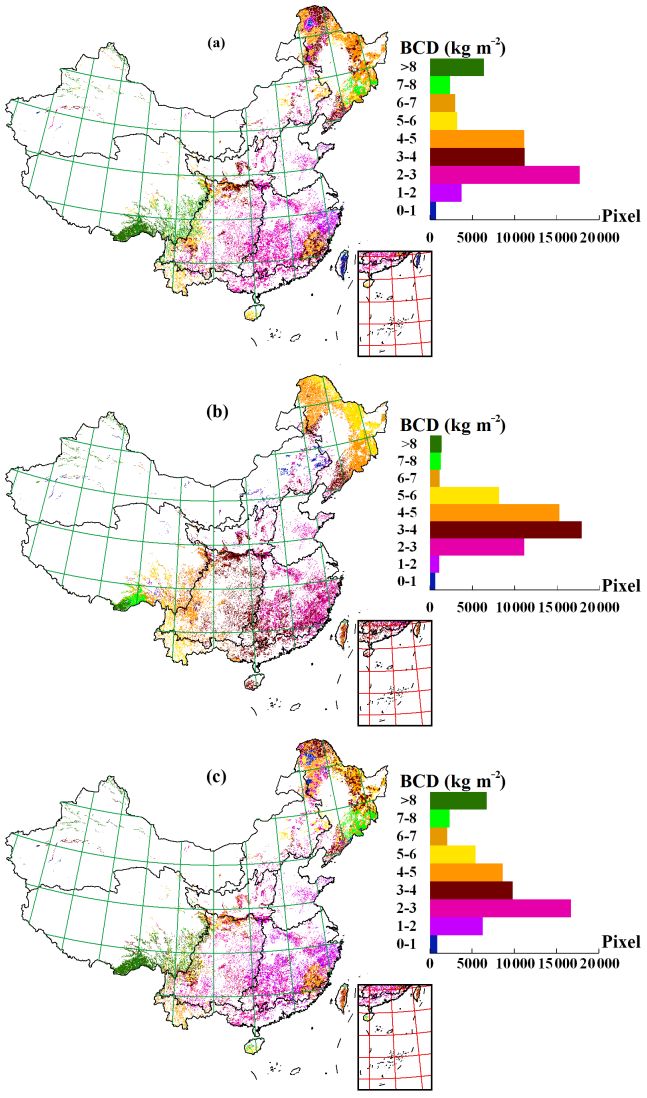

Figure 3. The spatial distribution of forest biomass BCDs estimated during the period 2004–2008 in China using **(a)** Kriging, **(b)** SOA, and **(c)** HASM-S.

increased from 0.63 Pg in period 1 to 1.84 Pg in period 5, and the BCSs for deciduous broad-leaved forests rose from 1.38 Pg in period 1 to 2.11 Pg in period 5. These trends can be modelled with the following regression equations:

$$\mathrm{BCS}_1(t) = 0.312t + 0.286, \quad R = 0.998, \tag{11}$$

$$\mathrm{BCS}_2(t) = 0.199t + 1.115, \quad R = 0.981, \tag{12}$$

where t corresponds to period t, $t = 1$, 2, 3, 4, and 5; $\mathrm{BCS}_1(t)$ and $\mathrm{BCS}_2(t)$ are, respectively, the BCSs of evergreen broad-leaved forests and deciduous broad-leaved forests in the period t and R represents the correlation coefficient of the corresponding regression equation.

The BCSs of deciduous coniferous forests fluctuated from period to period. Evergreen coniferous forests and broad-leaved and coniferous mixed forests exhibited an increasing trend of BCS in general but declined in period 3. Their trends were modelled with the following regression equations:

$$\mathrm{BCS}_3(t) = 0.207t + 1.391, \quad R = 0.932, \tag{13}$$

$$\mathrm{BCS}_4(t) = 0.076t - 0.068, \quad R = 0.867, \tag{14}$$

where t corresponds to periods 1, 2, 3, 4 and 5; $\mathrm{BCS}_3(t)$ represents the BCSs of evergreen coniferous forests in the period t; $\mathrm{BCS}_4(t)$ refers to the broad-leaved and coniferous mixed forests, and R represents the correlation coefficient of the corresponding regression equation.

Equations (8), (9), and (10) indicate that increasing rates of BCS, BCD, and FA were 0.531 Pg, 0.125 kg m^{-2}, and 0.083 million km^2 respectively over a 5-year period on average. According to Eqs. (11) and (12), the BCS of evergreen broad-leaved forests had a growth rate of 0.312 Pg over a 5-year period, which was 0.113 Pg higher than that for deciduous broad-leaved forests because of the different increasing rates of BCD; the BCD of evergreen broad-leaved forests increased by 1.87 kg m^{-2}, while the BCD of deciduous broad-leaved forests increased by 0.18 kg m^{-2} from periods 1 to 5. Equations (13) and (14) show that carbon stocks of evergreen coniferous forests grew much faster than those for broad-leaved and coniferous mixed forests. The former grew by 0.207 Pg but the latter by only 0.076 Pg in a 5-year period on average because the area of evergreen coniferous forests was 5 times larger (0.50×10^6 km^2 compared to 0.09×10^6 km^2 for broad-leaved and coniferous mixed forests) and offset the lower BCD growth rate of the former (0.132 kg m^{-2}) compared to 0.56 kg m^{-2} for broad-leaved and coniferous mixed forests per 5-year period.

The results from Kriging and HASM-S exhibit a similar spatial pattern on the national level, especially in southern Tibet, the Xiao Hinggan Mountains, the Changbai Mountains, and southern China. Some differences occur in Taiwan and Xinjiang as well as the Qinling Mountains. Compared to HASM-S, Kriging is strongly influenced by sample-plot density. The spatial heterogeneity of the results from SOA is not so obvious because NDVI, a critical variable of SOA, is not so sensitive to a change of carbon stocks, especially in northeastern China and near the lower reaches of Yangtze River.

The scatter diagrams of simulated BCD against observed BCD (Fig. 6) indicate that the BCD surface created by Kriging exhibits a higher correlation with observed BCD, $R^2 = 0.826$. However, the Kriging interpolation generated large errors in the Xizang/Tibet and Xinjiang regions, which have the highest BCD. The BCD was overestimated in Xizang and underestimated in Xinjiang. The BCD surface created by SOA has the lowest coefficient of determination, $R^2 = 0.627$, with the observed BCD surface. The SOA results show that BCDs in higher and lower latitudes are larger than those in middle latitudes except for Xinjiang and Xizang. The BCD was overestimated in Xinjiang but underestimated in Xizang. The surface of BCDs generated by HASM-S has the best corre-

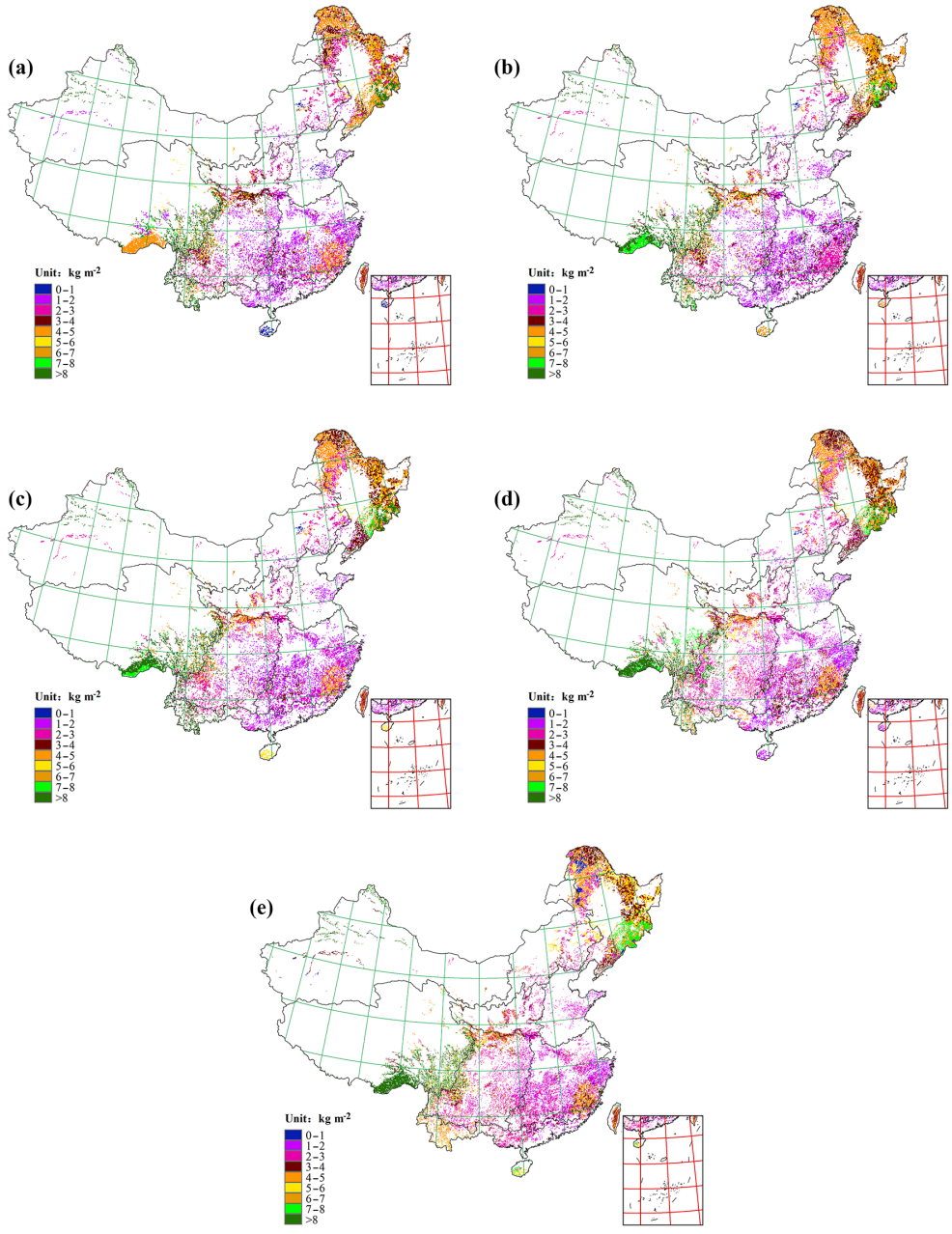

Figure 4. The spatial distribution of forest BCDs in China estimated during the five periods using HASM-S: **(a)** 1984–1988 (P1), **(b)** 1989–1993 (P2), **(c)** 1994–1998 (P3), **(d)** 1999–2003 (P4), and **(e)** 2004–2008 (P5).

lation with the surface of observed BCDs, $R^2 = 0.943$, and it generated the smallest errors in the regions of Xizang and Xinjiang compared to the other methods.

5 Discussion and conclusions

HASM-S overcame the shortcomings of both the ground-based national forest inventory and the satellite remote-sensing observations by fusing information about the details of the carbon stocks observed on the Earth's surface and the variability of the carbon surface observed from space. The cross-validation demonstrated that HASM-S was 26.1 % more accurate than the satellite-based approach and 28.4 % more accurate than spatial interpolation of the sample plots. These findings suggest that China's forest BCSs are more likely to be closer to our estimates than those generated by past efforts to estimate these same carbon stocks and their change over time.

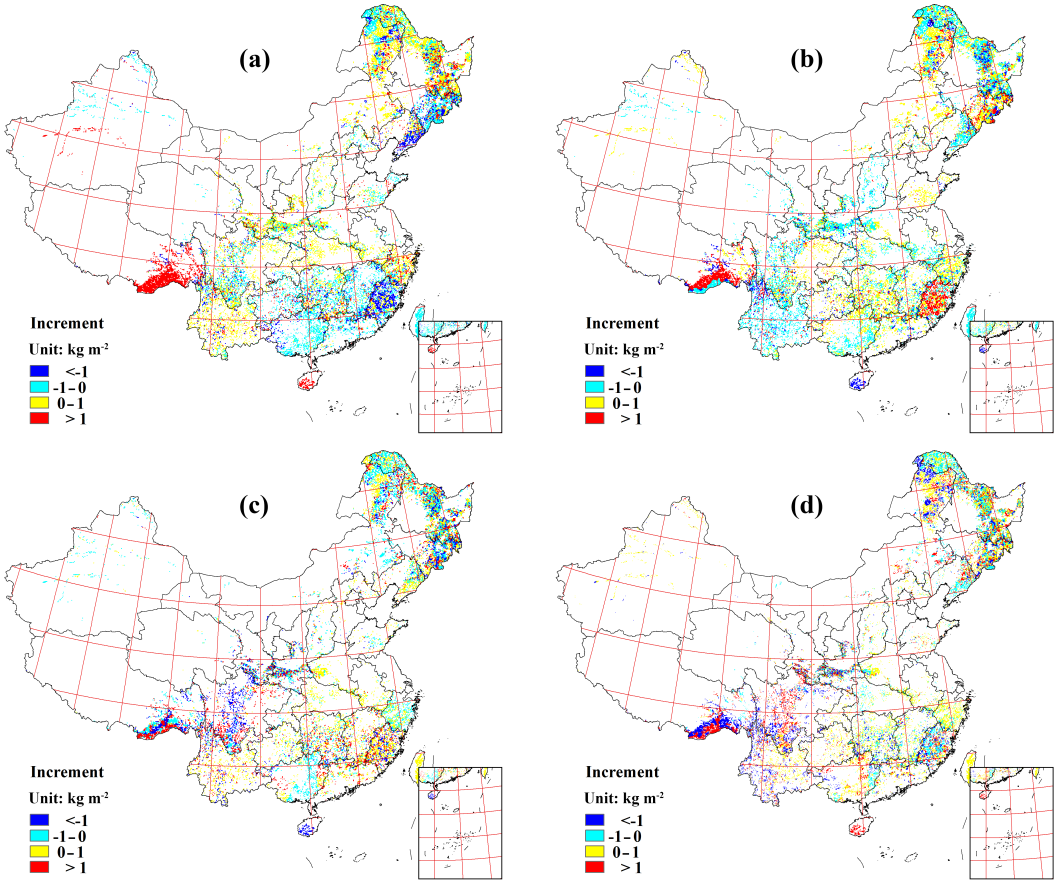

Figure 5. The increment maps of biomass carbon stocks from comparing two adjacent periods: **(a)** BCS in Period 2 minus BCS in Period 1, **(b)** BCS in Period 3 minus BCS in Period 2, **(c)** BCS in Period 4 minus BCS in Period 3, and **(d)** BCS in Period 5 minus BCS in Period 4.

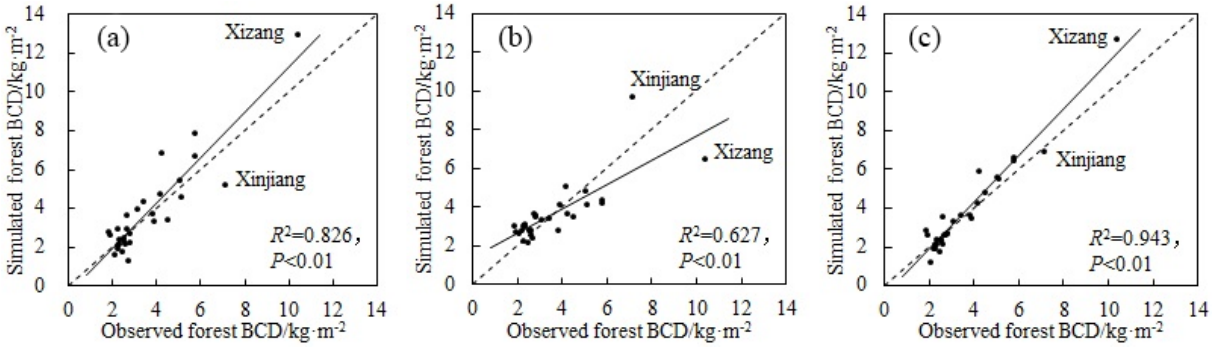

Figure 6. The scatter diagrams of simulated BCD against observed BCD: **(a)** Kriging, **(b)** SOA, and **(c)** HASM-S.

Taken as a whole, the HASM-S results show that the forest carbon stocks of China have increased by 2.24 Pg during the period 1984–2008 to a new high of 7.08 Pg C in 2008. These numbers fall in the middle of the previously published estimates. All of the estimates show forest BCSs in China increasing from 1973 to 2008, notwithstanding the various methods used and the varying levels of uncertainty embedded in these different methods and the data sources used.

The results from HASM-S compare favourably with those of other studies. For instance, the annual growth of total BCS from period 1 (circa 1986) to period 5 (circa 2006) in China was 0.112 Pg C yr^{-1}. This estimate was higher than that of Zhang et al. (2013), which was 0.103 Pg C yr^{-1}. However, our estimate of 0.148 Pg C yr^{-1} from period 3 (circa 1996) to period 5 (circa 2006) was lower than the 0.174 PgCyr^{-1} estimated by Zhang et al. (2013). From period 4 (circa 2001)

to period 5 (circa 2006), the 0.14 $PgCyr^{-1}$ estimated by HASM-S was twice that estimated by Liu et al. (2015).

In recent years, there are several different vegetation biomass maps for pantropical areas (e.g. Avitabile et al., 2016; Baccini et al., 2012; Saatchi et al., 2011). They were based on a combination of data from ground observations and satellite remote sensing. The spatial distribution pattern of the forest biomass carbon at low latitudes of China area simulated by HASM-S was generally consistent with the biomass carbon maps for pantropical areas, i.e. south of the Tibetan Plateau had the highest biomass carbon density, followed by the southeastern Tibetan Plateau, west of the Yunnan–Guizhou Plateau, the area of Qinling Mountains, and the Daba Mountains; southeastern China has the lowest forest biomass density except the area of Wuyi Mountains. However, the biomass carbon densities from HASM-S were lower than the one from Baccini et al. (2012), especially in southeastern China.

The Grain for Green program, which was launched in 1999 and aims to restore the country's forests and grasslands to prevent soil erosion, has emerged as one of the key drivers of carbon sequestration in China. The increase in forest growth rate under climate change may also contribute to sequestering more carbon, but it has relatively less impact than the restoration of forest lands or establishment of new forests (Forte, 2009). This program targets land with slopes $>25°$ (Xu et al., 2006; Yue et al., 2010c) and has been implemented in four phases: (1) a pilot phase (1999–2001), (2) an initial construction phase (2002–2010), (3) a consolidation phase (2011–2013), and (4) a second construction phase to be built around a new round of Grain for Green program expenditures (2014–2020).

The pilot program launched in 1999 focused on three provinces: Gansu, Shaanxi, and Sichuan. Approximately 381 000 ha of farmland was converted into forestland and 66 000 ha of bare land was reforested. In 2000, the program was expanded to 17 provinces, and the converted farmland and reforested bare land totals grew to 410 000 and 449 000 ha respectively. By 2001, 20 provinces were involved in the program and 420 000 and 563 000 ha of farm and bare land had been reforested respectively (Table 5). The national Grain for Green program was launched in China in 2002 and, by the end of 2010, 14.667 million ha of farmland had been converted to forest or grassland and 17.333 million ha of bare land had been reforested. During the consolidation phase from 2011 to 2013, scientific monitoring and management of the converted and reforested lands was strengthened to help sustain the aforementioned achievements of the Grain for Green program over the long term.

To grow and consolidate these gains, the potential for farmland conversion at the county level during the period 2014–2020 was estimated in 2014 by counting up farmers' voluntary applications to determine how large an area could be converted to forest or grassland. By 2020, 2.827 million ha of farmland could be converted, which includes 1.449 million ha of farmland with slopes $>25°$, 1.133 million ha of cultivated land threatened by desertification, and 247 000 ha of farmland with slopes between 15 and 25° around the Danjiangkou and Three Gorges reservoirs.

Table 5. Converted farmland and reforested bare land included in China's Grain for Green Program (millions hectares) (Office of Converting Farmland to Forestry, State Forestry Administration of China, 2014, 2016).

Year	Converted farmland	Afforestation on bare land	Total
1999	0.381	0.066	0.448
2000	0.405	0.468	0.872
2001	0.42	0.563	0.983
2002	2.647	3.082	5.729
2003	3.367	3.767	7.133
2004	0.667	3.333	4
2005	1.114	1.321	2.435
2006–2010	5.666	4.733	10.4
2014	0.333		0.333
2015	0.667		0.667
1999–2015	15.667	17.333	33
2016–2020	1.827		1.827

The results from this latest phase of the Grain for Green program are encouraging. Participating farmers can choose whether farmland is to be converted to forest or grassland and which species will be planted, and they will receive a CNY 22 500 subsidy for every hectare of farmland converted to forest or grassland. In 2014, 322 000 ha were converted to forest and 11 000 ha were converted to grassland, and in 2015 another 667 000 ha of farmland will be converted to either forest or grassland.

The BCS growth was improved by already existing forests and newly planted forests. The former accounted for about 55 % while the latter about 40 %. The BCS in existing forests had a growth rate of about 0.55 $kg\,m^{-2}$ per 5-year period and the BCS in newly planted forests grew at 1.8 $kg\,m^{-2}$ per 5-year period.

Methodologically the fusion of forest inventory data with satellite observations achieved with HASM-S provided much more accurate estimates of forest BCSs and their changes (Yue et al., 2016). This kind of method can increase our understanding of the role of forests in the carbon cycle and help to support greenhouse gas inventories and terrestrial carbon accounting projects (Muukkonen and Heiskanen, 2007).

However, HASM-S still has some limitations. (1) It can only simulate a surface of carbon stocks at a specific time or the average condition for a period when there are ground observations; in other words, it is difficult to use this approach to estimate changes at higher temporal resolutions. (2) It cannot generate and capture the likely impacts of future interventions and scenarios. For finding solutions to these limitations, we aim to develop a method for data assimilation

which combines HASM and the Dynamic Global Vegetation Model developed jointly by Lund University, Potsdam Institute for Climate Impact Research, and the Max Planck Institute for Biogeochemistry Jena (LPJ-DGVM) (Sitch et al., 2003), so that surfaces of carbon stocks could be simulated with less uncertainty in time series ranging from the past to the present and for user-specified periods in the future. Future research should aim at improving uncertainty estimates by deriving confidence intervals in the estimated carbon stocks by applying the basic principles of sampling theory and/or using models that contains the code for uncertainty analysis, such as the Monte Carlo approach. Uncertainty estimates can allow decision makers to better appreciate the amplitude of the errors in carbon stock estimates. For researchers, uncertainty estimates may contribute to improving methodologies to estimate carbon stocks.

Appendix A: List of abbreviations

Abbreviation	Explanation
BCD	Biomass carbon density
BCS	Biomass carbon stock
BEF	Biomass expansion factor (method)
CBM	Continuous BEF method
CF	Carbon factor
DGVM	Dynamic Global Vegetation Model
EOS	Earth Observation System
FA	Forest area
FID	Forestry inventory database
HASM	High-accuracy surface modelling (method)
LPJ	Lund University, Potsdam Institute for Climate Impact Research and Max Planck Institute for Biogeochemistry, Jena
MAE	Mean absolute error
MBCD	Mean biomass carbon density
MBD	Mean biomass density
MRE	Mean relative error
MODIS	Moderate Resolution Imaging Spectroradiometer
MR	Mean ratio
NDVI	Normalized Difference Vegetation Index
NPP	Net primary productivity
SOA	Satellite-observation-based approach

The Supplement related to this article is available online at doi:10.5194/bg-13-3991-2016-supplement.

Acknowledgements. This work was supported by the National Natural Science Foundation of China (91325204), by the National High-tech R&D Program of the Ministry of Science and Technology of the People's Republic of China (2013AA122003), and by the National Basic Research Priorities Program (2010CB950904) of the Ministry of Science and Technology of the People's Republic of China.

Edited by: M. Dai

References

Ahlstroem, A., Schurgers, G., Arneth, A., and Smith, B.: Robustness and uncertainty in terrestrial ecosystem carbon response to CMIP5 climate change projections, Environ. Res. Lett., 7, 044008, doi:10.1088/1748-9326/7/4/044008, 2012.

Avitabile, V., Herold, M., Heuvelink, G. B. M. et al.: An integrated pan-tropical biomass maps using multiple reference datasets, Glob. Change Biol., 22, 1406–1420, 2016.

Baccini, A., Goetz, S. J., Walker, W. S., Laporte, N. T., Sun, M., Sulla-Menashe, D., J. Hackler, Beck, P. S. A., Dubayah, R., Friedl, M. A., Samanta, S., and Houghton, R. A.: Estimated carbon dioxide emissions from tropical deforestation improved by carbon-density maps, Nature Climate Change, 2, 182–185, 2012.

Barman, R., Jain, A. K., and Liang, M. L.: Climate-driven uncertainties in modeling terrestrial gross primary production: A site level to global-scale analysis, Glob. Change Biol., 20, 1394–1411, 2014.

Canadell, J. G. and Raupach, M. R.: Managing forests for climate change mitigation, Science, 320, 1456–457, 2008.

Chen, C. F. and Yue, T. X.: A method of DEM construction and related error analysis, Comput. Geosci., 36, 717–725, 2010.

Chen, C. F., Li, Y. Y., and Yue, T. X.: Surface modeling of DEMs based on a sequential adjustment method, Int. J. Geogr. Inf. Sci., 27, 1272–1291, 2013b.

Chen, C. F., Yue, T. X., Dai, H. L., and Tian, M. Y.: The smoothness of HASM, Int. J. Geogr. Inf. Sci. 27, 1651–1667, 2013a.

Deng, S. H., Shi, Y. Q., Jin, Y., and Wang, L. H.: A GIS-based approach for quantifying and mapping carbon sink and stock values of forest ecosystem: A case study, Energy Procedia, 5, 1535–1545, 2011.

Editorial Committee of Vegetation Map of China: Vegetation Map of the People's Republic of China, Geological Publishing House, Beijing, 2007 (in Chinese).

Fang, J. Y., Guo, Z. D., Piao, S. L., and Chen, A. P.: Terrestrial vegetation carbon sinks in China, 1981–2000, Sci. China Earth Sci., 50, 1341–1350, 2007.

Forte, R. W.: Carbon sequestration in forests, Congressional Research Service Report for Congress 7-5700, 23 pp., 2009.

Gonzalez-Benecke, C. A., Martin, T. A., Cropper Jr., W. P., and Bracho, R.: Forest management effects on in situ and ex situ slash pine forest carbon balance, Forest Ecol. Manage., 260, 795–805, 2010.

Guo, Z. D., Fang, J. Y., Pan, Y. D., and Birdsey, R.: Inventory-based estimates of forest biomass carbon stocks in China: A comparison of three methods, Forest Ecol. Manage., 259, 1225–1231, 2010.

Hulme, M., Conway, D., Jones, P. D., Jiang, T., Barrow, E. M., and Turney, C.: Construction of a 1961–1990 European climatology for climate change modelling and impact applications, Int. J. Climatol., 15, 1333–1363, 1995.

Jung, J., Kim, S., Hong, S., Kim, K., Kim, E., Im, J., and Heo, J.: Effects of national forest inventory plot location error on forest carbon stock estimation using k-nearest neighbor algorithm, ISPRS J. Photogramm., 81, 82–92, 2013.

Li, H. K. and Lei, Y. C.: Estimation and Evaluation of Forest Biomass Carbon Storage in China, China Forestry Press, Beijing, 2010 (in Chinese).

Liu, Y. Y., van Dijk, A. I. J. M., de Jeu, R. A. M., Canadell, J. G., McCabe, M. F., Evans, J. P., and Wang, G.J.: Recent reversal in loss of global terrestrial biomass, Nature Climate Change, 5, 470–474, 2015.

Muukkonen, P. and Heiskanen, J.: Biomass estimation over a large area based on standwise forest inventory data and ASTER and MODIS satellite data: A possibility to verify carbon inventories, Remote Sens. Environ., 107, 617–624, 2007.

Ni, J.: Carbon storage in Chinese terrestrial ecosystems: Approaching a more accurate estimate, Climatic Change, 119, 905–917, 2013.

Office of Converting Farmland to Forestry, State Forestry Administration of China: A new round of the overall concept of returning farmland to forest and grass, Newsletter for Converting Farmland to Forestry, 194, 1–2, 2014 (in Chinese).

Office of Converting Farmland to Forestry, State Forestry Administration of China: New Year's Speech, Newsletter for Converting Farmland to Forestry, 198, 1–2, 2016 (in Chinese).

Piao, S. L., Fang, J. Y., Zhu, B., and Tan, K.: Forest biomass carbon stocks in China over the past 2 decades: Estimation based on integrated inventory and satellite data, J. Geophys. Res., 110, G01006, doi:10.1029/2005JG000014, 2005.

Piao, S. L., Fang, J. Y., Ciais, P., Peylin, P., Huang, Y., Sitch, S., and Wang, T.: The carbon balance of terrestrial ecosystems in China, Nature, 458, 1009–1014, 2009.

Prentice, I. C., Farquhar, G. D., Fasham, M. J. R. et al.: The carbon cycle and atmospheric carbon dioxide, in: Climate Change 2001: The Scientific Basis, edited by: Houghton, J. T., Ding, Y., Griggs, D. J., Noguer, M., Van Der Linden, P. J., Dai, X., Maskell, K., and Johnson, C. A., Cambridge, Cambridge University Press, 183–237, 2001.

Saatchi, S. S., Harris, N. L., Brown, S., Lefsky, M., Mitchard, E.T.A., Salas, W., Zutta, B. R., Buermann, W., Lewis, S. L., Hagen, S., Petrova, S., White, L., Silman, M., and Morel, A.: Benchmark map of forest carbon stocks in tropical regions across three continents, P. Natl. Acad. Sci., 108, 9899–9904, 2011.

Shi, W. J., Liu, J. Y., Song, Y. J., Du, Z. P., Chen, C. F., and Yue, T. X.: Surface modeling of soil pH, Geoderma, 150, 113–119, 2009.

Sitch, S., Smith, B., Prentice, I. C., Arneth, A., Bondeau, A., Cramer, W., Kaplan, J. O., Levis, S., Lucht, W., Sykes, M. T., Thonicke, K., and Venevsky, S.: Evaluation of ecosystem dynamics, plant geography and terrestrial carbon cycling in the LPJ Dy-

namic Global Vegetation Model, Glob. Change Biol. 9, 161–185, 2003.

State Forestry Administration of China: National Forest Report (2004–2008), China Forestry Publishing House, Beijing, 2009 (in Chinese).

Thurner, M., Beer, C., Santoro, M., Carvalhais, N., Wutzler, T., Schepaschenko, D., Shvidenko, A., Kompter, E., Ahrens, B., Levick, S. R., and Schmullius, C.: Carbon stock and density of northern boreal and temperate forests, Global Ecol. Biogeogr., 23, 297–310, 2014.

Wang, S., Chen, J. M., Ju, W. M., Feng, X., Chen, M., Chen, P., and Yu, G.: Carbon sinks and sources in China's forests during 1901–2001, J. Environ. Manage., 85, 524–537, 2007.

Xu, Z. G., Xu, J. T., Deng, X. Z., Huang, J. K., Uchida, E., and Rozelle, S.: Grain for Green versus grain: Conflict between food security and conservation set-aside in China, World Development, 34, 130–148, 2006.

Yang, K. and Guan, D. S.: Changes in forest biomass carbon stock in the Pearl River Delta between 1989 and 2003, J. Environ. Sci., 20, 1439–1444, 2008.

Yu, G. R., Chen, Z., Piao, S. L., Peng, C. H., Ciais, P., Wang, Q. F., Li, X. R., and Zhu, X. J.: High carbon dioxide uptake by subtropical forest ecosystems in the East Asian monsoon region, P. Natl. Acad. Sci. USA, 111, 4910–4915, 2014.

Yue, T. X.: Surface Modelling: High Accuracy and High Speed Methods, CRC Press, Boca Raton, FL, 2011.

Yue, T. X. and Wang, S. H.: Adjustment computation of HASM: A high-accuracy and high-speed method, Int. J. Geogr. Inf. Sci., 24, 1725–1743, 2010.

Yue, T. X., Du, Z. P., Song, D. J., and Gong, Y.: A new method of surface modeling and its application to DEM construction, Geomorphology, 91, 161–172, 2007.

Yue, T. X., Chen, C. F., and Li, B. L.: An adaptive method of high accuracy surface modeling and its application to simulating elevation surfaces, Transactions in GIS, 14, 615–630, 2010a.

Yue, T. X., Song, D. J., Du, Z. P., and Wang, W.: High-accuracy surface modelling and its application to DEM generation, Int. J. Remote Sens., 31, 2205–2226, 2010b.

Yue, T. X., Wang, Q., Lu, Y. M., Xin, X. P., Zhang, H. B., and Wu, S. X.: Change trends of food provisions in China, Global Planet Change, 72, 118–130, 2010c.

Yue, T. X., Chen, C. F., and Li, B. L.: A high accuracy method for filling SRTM voids and its verification, Int. J. Remote Sens., 33, 2815–2830, 2012.

Yue, T. X., Zhao, N., Yang, H., Song, Y. J., Du, Z. P., Fan, Z. M., and Song, D. J.: The multi-grid method of high accuracy surface modelling and its validation, Transactions in GIS, 17, 943–952, 2013a.

Yue, T. X., Zhao, N., Ramsey, R. D., Wang, C. L., Fan, Z. M., Chen, C. F., Lu, Y. M., and Li, B. L.: Climate change trend in China, with improved accuracy, Climate Change, 120, 137–151, 2013b.

Yue, T. X., Du, Z.P., Lu, M., Fan, Z. M., Wang, C. L., Tian, Y. Z., and Xu, B.: Surface modelling of ecosystem responses to climatic change, Ecol. Modell., 306, 16–23, 2015a.

Yue, T. X., Zhao, M. W., and Zhang, X. Y.: A high-accuracy method for filling voids on remotely sensed XCO_2 surfaces and its verification, J. Clean. Prod., 103, 819–827, 2015b.

Yue, T. X., Zhang, L. L., Zhao, N., Zhao, M. W., Chen, C. F., Du, Z. P., Song, D. J., Fan, Z. M., Shi, W. J., Wang, S. H., Yan, C. Q., Li, Q. Q., Sun, X. F., Yang, H., Wang, C. L., Wang, Y. F., Wilson, J. P., and Xu, B.: A review of recent developments in HASM, Environ. Earth Sci., 74, 6541–6549, 2015c.

Yue, T. X., Liu, Y., Zhao, M. W., Du, Z. P., and Zhao, N.: A fundamental theorem of Earth 's surface modelling, Environ. Earth Sci., 75, 1–12, 2016.

Zhang, C. H., Ju, W. M., Chen, J. M., Zan, M., Li, D. Q., Zhou, Y. L., and Wang, X. Q.: China's forest biomass carbon sink based on seven inventories from 1973 to 2008, Climatic Change, 118, 933–948, 2013.

Zhao, N. and Yue, T. X.: A modification of HASM for interpolating precipitation in China, Theor. Appl. Climatol., 116, 273–285, 2014a.

Zhao, N. and Yue, T. X.: Sensitivity studies of a high accuracy surface modelling method, Science China-Earth Science, 57, 1–11, 2014b.

Zhou, L. S., Sun, H., Shen, Y. Q., Deng, J. Z., and Shi, Y. L.: Comprehensive Agricultural Planning of China, China Agricultural Press, Beijing, 1981 (in Chinese).